Phys. Status Solidi B, 1–4 (2016) / **DOI** 10.1002/pssb.201600247

physica status solidi b
www.pss-b.com
basic solid state physics

Scattering near-field optical microscopy on metallic and semiconducting carbon nanotube bundles in the infrared

Gergely Németh*, Dániel Datz, Hajnalka M. Tóháti, Áron Pekker, and Katalin Kamarás

Institute for Solid State Physics and Optics, Wigner Research Centre for Physics, Hungarian Academy of Sciences, Budapest, Hungary

Received 19 April 2016, revised 25 May 2016, accepted 2 June 2016
Published online 29 June 2016

Keywords nanotubes, near-field infrared microscopy, s-SNOM

* Corresponding author: e-mail nemeth.gergely@wigner.mta.hu, Phone: +36-1-3922222, Fax: +36-1-3922219

We demonstrate that scattering-type near-field optical microscopy (s-SNOM) at infrared frequencies can be effectively used to distinguish between carbon nanotube (CNT) bundles based on their electrical properties. Samples from separated metallic and semiconductor nanotubes and their mixtures were investigated using infrared lasers under near-field conditions. In this frequency range, the difference in the free-carrier concentration between metallic and semiconducting tubes is expected to influence the properties of the scattered light. The remarkable difference in the optical phase images proves that this is indeed the case: the metallic and semiconducting bundles are unambiguously identifiable in the sample, even in case of 5 nm diameter bundles. The measurements agree qualitatively with our calculations based on the extended finite dipole model using the known optical functions of the constituting nanotubes.

1 Introduction The extension of near-field optical microscopy into the infrared has been an exciting development in optical imaging, since the spatial resolution was reduced to orders of magnitude below the diffraction limit [1–3]. Scattering-type scanning near-field optical microscopy (s-SNOM) yields information on the optical characteristics from the scattered light enhanced by a strong, localized electromagnetic field between a metal-coated tip and the sample. The spatial resolution of the infrared s-SNOM method is 20–50 nm, the size of typical bundles consisting of single-walled carbon nanotubes (SWCNTs) [4]. The electronic structure and optical properties of SWCNTs are influenced by their chirality. In samples separated by electronic type [5] (metallic or semiconducting), bundles are supposed to be homogeneous and the low-frequency optical properties, determined by the free-carrier concentration, should indicate the electronic type.

We demonstrate here that scattering-type near-field optical microscopy at infrared frequencies is indeed capable of distinguishing semiconducting from metallic SWCNT bundles; in a proof-of-principle experiment, we also show that in a mixture of homogeneous bundles down to the size of a few nanometers, the two types of SWCNTs can be localized. Our findings are supported by model calculations.

2 Experimental methods

2.1 Sample preparation We acquired high purity, (95%) single-walled nanotube suspensions from NanoIntegris, Inc. separated by density gradient ultracentrifugation (Isonanotube-M,S) [6]. We sonicated the nanotube suspension to reduce the size of the bundles. Thin films were prepared by vacuum filtration using acetone soluble filter membranes. The membranes were dissolved in boiling acetone, and the films were transferred to a silicon substrate [7]. The CNT-Si samples were then washed in ethanol and isopropyl alcohol. Three different samples were produced using this technique; one pure semiconducting, one pure metallic and one mixture (50–50%). In the case of the mixed sample, after sonication, the suspensions were mixed, followed by filtering and rinsing with water. This way, we made sure that the majority of the bundles constituting the film was composed of either only metallic or only semiconducting nanotubes.

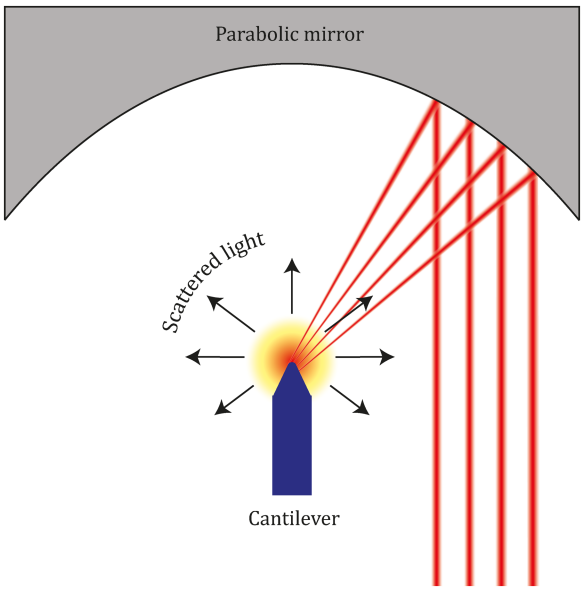

Figure 1 Schematic top-view of the s-SNOM experiment. The parabolic mirror is used both to focus the laser beam to the apex of the tip and to collect the scattered light.

2.2 Scattering-type SNOM The s-SNOM setup is based on an atomic force microscope (AFM) combined with an asymmetric Michelson interferometer. The tip is illuminated by a focused laser beam, generating an enhanced and localized optical near field at the tip apex, used as an ultra-small light source to locally probe the sample (Fig. 1). Because of the interaction between the tip and the sample, the scattered light contains information about the local optical properties [8]. In the experiments, we used a neaSNOM Microscope (neaspec GmbH, www.neaspec.com) with platinum-coated tips. For the illumination, we applied an infrared quantum cascade laser (Daylight Solutions) at a frequency of 1000 cm^{-1} with a power about 2.7 mW. As infrared (IR) detector, we used a mercury cadmium telluride (MCT) detector. The AFM works in tapping mode with resonance frequency around 270 kHz at amplitude about 50 nm. The scattered light (E_s) is analyzed in the interferometer by pseudoheterodyne detection [8].

The measured signal will be proportional to the complex scattering coefficient (σ). The pseudoheterodyne detection and the demodulation of the signal at nth harmonics of the tip oscillation frequency yield the optical amplitude (s_n) and phase (φ_n) [9],

$$E_s = \sigma E_i \propto \sigma_n = s_n \cdot e^{i\varphi_n}. \tag{1}$$

This kind of detection is used to separate and accurately measure the near-field signal which would be obscured by the always present background signal that originates from the direct light scattering. In our measurements, we detected up to third harmonic amplitude (s_{O3}) and phase (φ_{O3}).

The total measurement time depends on the data acquisition time at one point and the pixel size of the image. Usual pixel time is 13 ms and for an image with size of 250 × 250 pixels. A full measurement takes around 15 min.

2.3 Analytical model In order to verify our predictions about the near-field signals of the different types of nanotubes, we made analytical calculations based on the extended finite dipole model (EFDM) [10]. This model approximates the scattered field with numerous dipoles and monopoles generated in the tip, in the substrate, and in the nanoparticle. We note that the incident electric field (E_0) is perpendicular to the substrate surface in the model. Owing to the elongated shape of the tip, the largest dipole moment can be generated in this direction in the tip, so the largest part of the near-field scattering comes from the normal component of the electric field [11].

The dipoles in the nanoparticle that were generated by the external electric field (E_0) were defined by the polarizability of the object. The original model uses a sphere, but in our case the nanotube bundles are more cylinder-like objects. In order to describe this situation, we simply exchanged the sphere with a cylinder by modifying the polarizability of the sphere to that of the cylinder. Polarizability of a cylinder with large aspect ratio can be approximated with the polarizability of a prolate ellipsoid, with large eccentricity ($e = \sqrt{1 - a_y^2/a_x^2}$, a_y and a_x being the semi-minor and semi-major axis of the spheroid). The following expression was introduced for the polarizability of an elongated cylinder perpendicular to its axis [12]:

$$\alpha_z = \frac{\epsilon - 1}{1 + N_z(\epsilon - 1)}, \tag{2}$$

$$N_z = N_y = \frac{1}{2}(1 - N_x),$$

$$N_x = \frac{1 - e^2}{2e^3}\left(\ln\frac{1+e}{1-e} - 2e\right),$$

N_z is the depolarization factor which can be calculated from the geometrical parameters of the cylinder. The depolarization factor measures the weakening of the internal field within the ellipsoid. In our experiments, the measured bundle diameters were around 5 nm, and the length of the bundles was more than 1 microns. Therefore, the eccentricity goes to zero, consequently $N_x = 0$ and $N_y = N_z = 1/2$. In Eq. (2), $\epsilon = \epsilon_1 + i\epsilon_2$ is the complex dielectric function of the cylinder's material, which is different for semiconducting and metallic SWNTs [13].

Figure 2 shows the charges of the EFDM model which mimic the electric field distribution around the apex of the tip. In the figure, E_0 represents the incident electric field, monopoles Q_0, Q_{ind} and dipoles P_1, P_2, P_3 describe the electric field of the tip, and p_0, p_1, p_2 stand for the field of the nanoparticle. Their mirror charges also exist in the substrate. The local electric field (E_{loc}) at the position of the dipole, and the polarizability (α_z) define the dipole moment as $p = \alpha_z E_{loc}$.

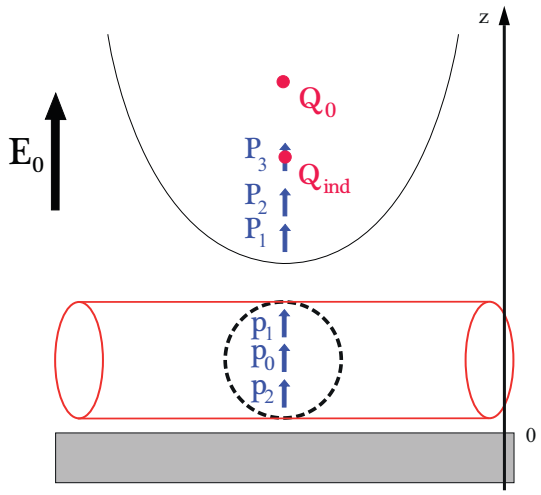

Figure 2 Schematic distribution of the charges used in EFDM model. The dipoles (p_0, p_1, p_2) describe the cylinder.

The complex dielectric functions we used were calculated from wide-range spectroscopy (far-infrared through ultraviolet) data via Kramers–Kronig analysis [14]. We have done the EFDM calculations around our laser frequency (1000 cm^{-1}). Figure 3a shows the complex dielectric function of the two type of nanotubes [13]. The imaginary part of the dielectric function of the metallic nanotubes is higher than that of the semiconducting tubes, therefore we expect a higher contrast relative to the substrate in the metallic case. The results of the EFDM calculations (Fig. 3b) confirm this expectation: the calculated phase signal for semiconducting nanotubes at the wavenumber of interest is near zero, whereas in case of the metallic nanotubes it is finite. Note that because of the simplicity of the model, this is only a qualitative result.

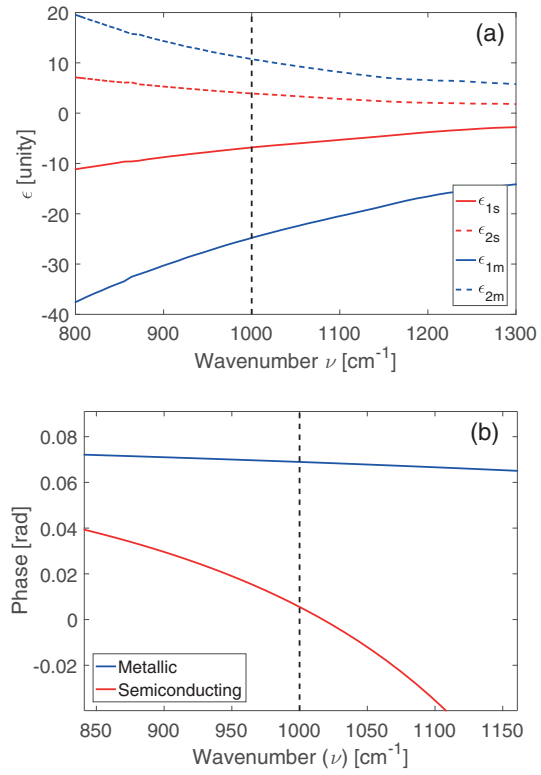

Figure 3 (a) The used dielectric function of metallic (blue), semiconducting (red) samples, (b) third harmonic near-field phase (φ_{O3}) of a nanotube bundle with $d = 6$ nm diameter calculated with EFDM model. (b) represents two calculations: metallic (blue), semiconducting (red), the vertical bar represents the frequency of the infrared laser used (black).

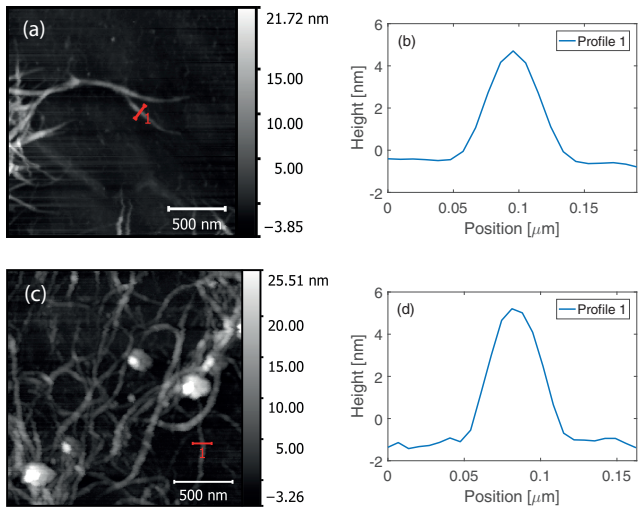

Figure 4 AFM topography images of the metallic (a), semiconducting (c) samples, and the corresponding line profiles across line 1, metallic (b), semiconducting (d).

3 Results and discussion First, we measured the enriched (95%) metallic and semiconducting nanotubes on silicon wafer, to determine if the method can distinguish between the two types of nanotubes in a reliable and reproducible way.

In order to obtain comparable optical signals, we had to search for bundles in each sample with the same bundle diameter. Figure 4 shows the chosen areas where we located a bundle in each sample with diameter $d \approx 5$–6 nm. While the lateral spatial resolution is lower than the diameter of our bundles, in the tangential direction (z-direction) the topography has the resolution of an AFM, and the optical signal above the nanotube bundle can be detected if its difference from the substrate signal overcomes the noise. The lateral resolution means that we cannot separate two bundles if they stay closer to each other than this value.

We note that all data were normalized to the signal of the silicon substrate. The substrate silicon was non-doped, and produced a spatially flat near-field signal.

In Fig. 5, we show spatial maps of the third-harmonic near-field amplitude for metallic (a) and semiconducting (c) tubes, respectively. We also present the third-harmonic phase maps for metallic (b) and semiconducting (d) samples. The amplitude contrasts of different electronic types of nanotubes are very similar, but the phase contrast is much more pronounced for metallic nanotubes than for semiconducting ones. The reason for this difference is that the effect

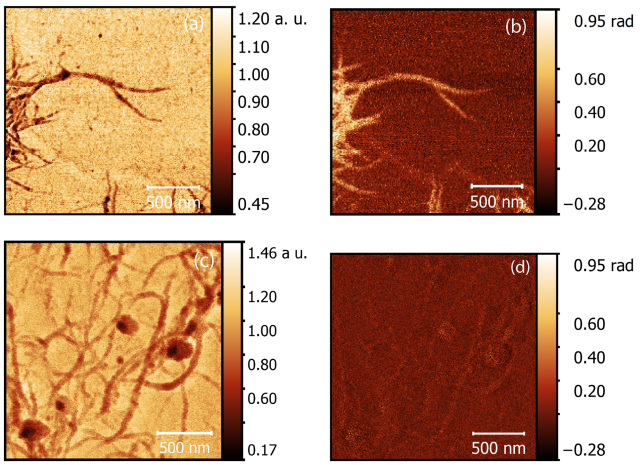

Figure 5 Third harmonic near-field amplitude and phase images of metallic (a,b) and semiconducting samples (c,d) at $\nu = 1000\,\mathrm{cm}^{-1}$.

of the imaginary part of the dielectric function on the phase is stronger than that of the real part on the amplitude. While the phase contrast between the silicon and the semiconducting bundles is almost zero, in the case of the metallic samples a phase contrast rises up to $\varphi \approx 22^{\circ} (\approx 0.38\,\mathrm{rad})$. This significant difference enables us to distinguish the electrically different nanotubes in a mixed or unknown sample.

In the final experiment, we made a mixture from the pure suspensions. The AFM topography of the transferred nanotubes is shown in Fig. 6. We chose two nanotube bundles with the same diameter $d \approx 4\,\mathrm{nm}$. The line profiles of these bundles are presented in Fig. 6.

On the optical phase maps (Fig. 7) which were taken simultaneously with the topography at $1000\,\mathrm{cm}^{-1}$ laser frequency, the two bundles noticeably differ from each other. As the line profiles that were extracted from the optical data show, the situation is the same as it was in the pure samples. The phase signal of the metallic bundles unambiguously rises above the substrate/background signal while the semiconducting ones stay hidden.

4 Conclusions and outlook We found that the difference in the free-carrier concentration of different nanotube bundles can cause significant phase shift in the scattered light. The optical phase images prove that the s-SNOM method

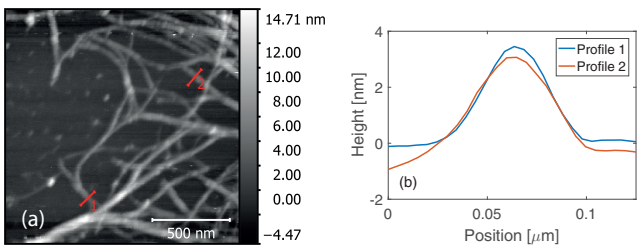

Figure 6 Topography of the mixed sample (SM) and the corresponding line profiles.

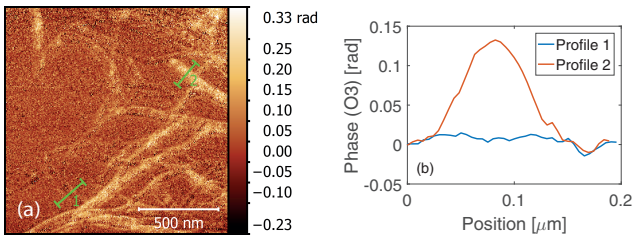

Figure 7 Third harmonic optical phase map of the area that contains both metallic and semiconducting bundles with similar diameters. All data were normalized to the silicon substrate.

is capable of distinguishing between metallic and semiconducting nanotube bundles in the mid-IR range. This method may work with smaller bundles size or single nanotubes, if the noise can be reduced further. We can experiment with other substrates to enhance the signal/noise ratio in order to probe single tubes. Furthermore, an interesting question is if the bundles contain both semiconducting and metallic CNTs. The question is that we could estimate what percentage of the bundle is semiconducting or metallic. This was not the object of these experiments now but it can be an interesting question to be answered in the future.

Acknowledgement Research supported by the Hungarian National Research Fund (OTKA) No. ANN 107580.

References

[1] R. Hillenbrand and F. Keilmann, Appl. Phys. Lett. **80**, 25–27 (2002).
[2] T. Taubner, R. Hillenbrand, and F. Keilmann, Appl. Phys. Lett. **85**, 5064–5066 (2004).
[3] J. M. Stiegler, Y. Abate, A. Cvitkovic, Y. E. Romanyuk, A. J. Huber, S. R. Leone, and R. Hillenbrand, ACS Nano **5**, 6494–6499 (2011).
[4] U. J. Kim, H. R. Gutiérrez, J. P. Kim, and P. C. Eklund, J. Phys. Chem. B **109**, 23358–23365 (2005).
[5] A. A. Green and M. C. Hersam, Nano Lett. **8**, 1417–1422 (2008).
[6] http://www.nanointegris.com/en/about-our-products
[7] Z. Wu, Z. Chen, X. Du, J. M. Logan, J. Sippel, M. Nikolou, K. Kamaras, J. R. Reynolds, D. B. Tanner, A. F. Hebard, and A. G. Rinzler, Science **305**, 1273–1276 (2004).
[8] N. Ocelic, A. Huber, and R. Hillenbrand, Appl. Phys. Lett. **89**, 101124 (2006).
[9] F. Keilmann and R. Hillenbrand, Nano-Optics and Near-Field Optical Microscopy (Artech House, Boston, 2009), chap. 11, pp. 235–265.
[10] A. Cvitkovic, Ph.D. thesis, Technische Universität München (2009).
[11] B. Knoll and F. Keilmann, J. Microsc. **194**, 512–515 (1999).
[12] J. Venermo and A. Sihvola, J. Electrostat. **63**, 101–117 (2005).
[13] H. M. Tóháti, Á. Pekker, B. Á. Pataki, Z. Szekrényes, and K. Kamarás, Eur. Phys. J. B **87**, 126 (2014).
[14] Á. Pekker and K. Kamarás, Phys. Rev. B **84**, 075475 (2011).

